# Spectra From Correlation

***Peter Morovič, Ján Morovič and Juan Manuel García–Reyero, Hewlett Packard Company, Sant Cugat del Vallés, Catalonia, Spain***

## Abstract

*Spectral reflectance is a key material property and contributor to object appearance. While it has long been known that reflectance in a given wavelength interval correlates strongly with reflectances in neighboring ones, this correlative property has only been exploited implicitly before. The present paper therefore presents a new approach to spectral analysis and synthesis that consists of first deriving a spectral correlation profile and then using it for a direct and full sampling of the spectral and color gamuts corresponding to it. The resulting technique can be used to generate natural-like spectra (or spectra following other, specific correlation properties) and it can also be incorporated into Bayesian models of spectral estimation.*

## Introduction

How much incident light an object reflects as a function of wavelength across the visible part of the electromagnetic spectrum is part of its material properties and also strongly influences its appearance. Consequently, spectral reflectances have been studied extensively from the perspectives of their dimensionality (Krinov, 1947; Cohen, 1964) or spectral and colorimetric gamuts (Chau and Cowan, 1996). Attempts have also been made to quantify the set of all natural reflectances (Schrödinger, 1920; Morovič *et al.*, 2012), to generate natural reflectances (Morovič and Finalyson, 2006) and to study them from the point of view of the human visual system's (HVS') evolution (Tkačik *et al.*, 2011).

Here, Tkačik *et al.* (2011) have collected a large set of calibrated and color-characterized images from the Okavango Delta of Botswana, which is like where the human eye is thought to have evolved. The study of these images indicates the constraints under which the HVS had to operate, such as what surface properties needed to be distinguished amongst on a physiological, pre-cortical level.

Brainard *et al.* (2006) then used such data and its properties to define a probabilistic model of human vision that was able to elegantly predict HVS behavior. Key to this model was a number of priors about the environment that surrounds us, such as the spatial correlation of sensor responses and the correlation of responses from different cone types. The analysis of a large quantity of both digital RGB images and LMS cone responses corresponding to them showed that RGBs in a pixel-level neighborhood correlate well with each other, meaning that spatial changes in a scene are typically gradual instead of abrupt, and that cone responses also change gradually, resulting in a good correlation of LMS responses.

Seeing the strong LMS correlations in the Brainard *et al.* paper lead to the question of whether these correlative relationships also hold at a lower – spectral – level, and whether it would therefore be possible to predict not cone responses or a dimensionally-reduced representation of reflectance spectra (Singh *et al.*, 2006), but to execute a Bayesian model directly in a reflectance domain, with appropriate reflectance priors. That such correlation is likely to be high is already implied in multivariate analysis, as will be shown in more detail later, and also in the analysis of hyperspectral data, where high spatial and spectral correlation is taken advantage of for the sake of data reduction and accelerated analysis (Smith *et al.*, 1985).

The following sections will therefore present an analysis of spectral correlation (which will be shown to be complementary to the multivariate analysis typically applied in this field), followed by a method for synthetizing natural spectra using the principle of correlation (which enables a direct, uniform sampling of spectral reflectance space that follows the distribution of a measured dataset), and finally a comparison of such correlation-synthetized spectra with measured spectra whose statistics they were designed to have. All of this will be in preparation for the correlation principle's future use both as a means of analysis and as a mechanism that can be integrated in Bayesian models.

## Spectral Correlation

In multivariate analysis the objective is to find the principal components of variation (cf. Morovič (2002) for a detailed analysis), which allows for a representation of the original data in a decorrelated way that therefore reduces its dimensionality. Instead, spectral correlation will here be looked at with the aim of preserving correlation and characterizing its specific behavior.

Spectral correlation is understood to be the relationship of $R(\lambda^i)$ against $R(\lambda^{i+1})$, where $R()$ denotes reflectance and $\lambda^i$ and $\lambda^{i+1}$ are the wavelengths of neighboring intervals in nanometers. Such relationships are easily visualized, with Fig. 1 showing them for the SOCS dataset of 53489 measured samples, with pseudo-colored dots indicating their respective wavelengths.

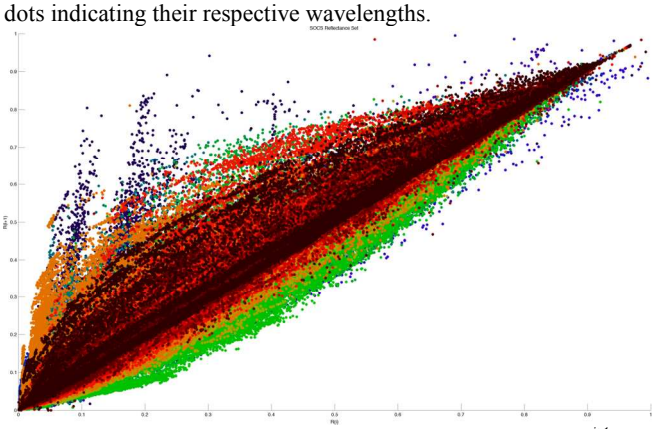

***Figure 1**. Correlation plot of the SOCS reflectance data set plotting $R(\lambda^{i+1})$ against $R(\lambda^i)$ with the dots' pseudo-colors indicating wavelength.*

A perfectly correlated data set would fall on the [0 1] diagonal line in the above plot and would only be possible for non-selective reflectances where $R(\lambda^i) = R(\lambda^{i+1})$. Fig. 1 clearly shows that the relationship between neighboring wavelengths is not arbitrary and also suggests that its nature may vary across the visible range. This is consistent with previous studies that have used multivariate analysis to show that the SOCS data can be well represented by 8-

 

13 linear bases, depending on whether the mean or the maximum reconstruction error is to be below 0.5 $\Delta E^*_{ab}$ (Kohonen, 2006).
It is also apparent from Fig. 1 that there are biases and outliers and that not all wavelengths have an equal spread along the diagonal axis. A wavelength-by-wavelength view (Fig. 2) shows the differences between individual correlations in more detail.

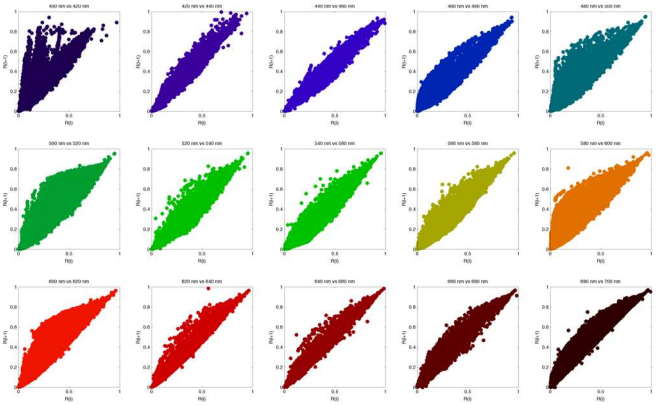

***Figure 2**. Correlation plot of the SOCS reflectance dataset plotting $R(\lambda^{i+1})$ against $R(\lambda^{i})$ for each wavelength from 400nm (showing the relationship between 400nm and 410nm) up to 690nm (showing the relationship between 690nm and 700nm) with dots pseudo-colored according to wavelength.*

For instance, there is a clear bias towards the upper-left triangle of the correlation plot, meaning that there are more cases where $R(\lambda^{i+1})$ has a larger reflectance than $R(\lambda^{i})$ compared to the opposite case. However, the above clearly contains noise, which can come either from the measurement process or from inconsistencies in the measured surfaces themselves, and is also dependent on spectral sampling (i.e., correlation between 1 nm intervals would be different than between 10 nm ones).

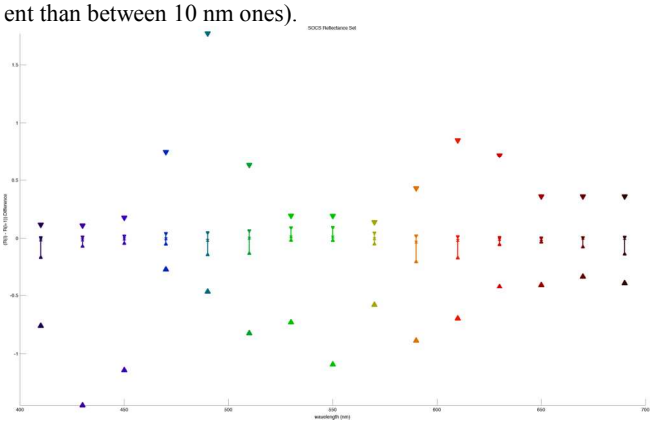

***Figure 3.** Per-wavelength view of the ranges between $R(\lambda^{i})$ and $R(\lambda^{i+1})$. Big upper and lower triangles show the min and max of the entire set, while smaller triangles connected by a line show the 90% of the range (removing the lower and upper 5% of data), with the median plotted as a cross on the line.*

To avoid over-analyzing the data, statistical filtering will be used to maintain a high percentage of the variation and discard upper and lower percentiles. Fig 3 shows the per-wavelength ranges of neighboring wavelength differences, $R(\lambda^{i}) - R(\lambda^{i+1})$, both based on all data (bigger lower and upper triangles) and on 90% of it (smaller triangles connected by a line) having discarded the top and bottom 5% on a per wavelength basis. A significant discrepancy can be seen here between the overall ranges and those obtained by removing the top/bottom 5% of the data (jointly accounting for 5349 sample points plotted in Figs. 1 and 2). Another insight is that the medians and the post-filtering min/max values are closely clustered around 0, which indicates a high probability of close to perfect correlation – zero here meaning no change from $R(\lambda^{i})$ to $R(\lambda^{i+1})$ and small absolute values representing a smooth change in reflectance. For a more complete view of the dataset, Fig. 4 shows its frequency histogram.

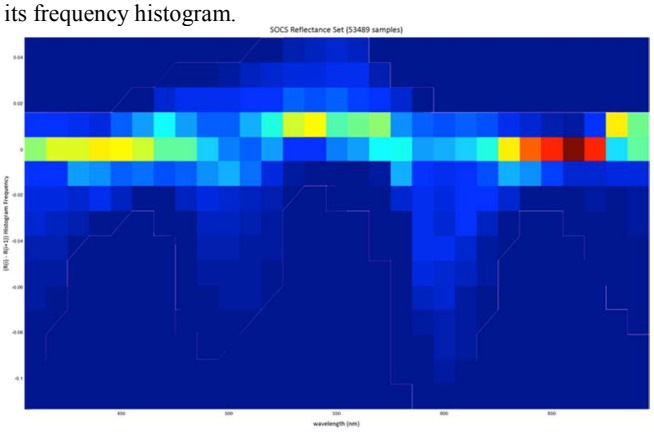


***Figure 4.** SOCS per-wavelength histogram of the range of differences between $R(\lambda^{i})$ and $R(\lambda^{i+1})$ without the top/bottom 5% of the difference data.*

After statistically filtering out the top and bottom 5% of neighboring wavelength interval differences, the remaining data is shown in Fig 5. Note, however, that this has no bearing on the reflectance synthesis method presented in the following section and only serves the purpose of discounting outliers upfront. A better understating of the source of outliers is planned for future work.

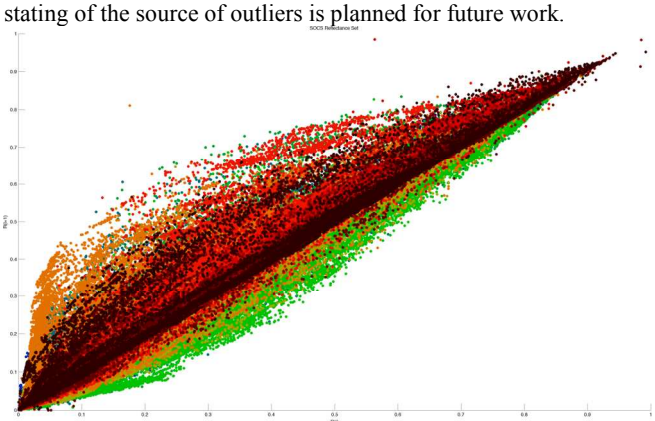

***Figure 5**. Correlation plot of the SOCS reflectance data after removing the top and bottom 5% of the range of differences per wavelength, plotting $R(\lambda^{i+1})$ against $R(\lambda^{i})$ with dots pseudo-colored depending on wavelength.*

To extend the above analysis, which has focused on the SOCS dataset, which is by far the largest of its kind in terms of the number of samples, Fig. 6 shows per-wavelength histograms of the range of differences for three other datasets: Westland (Westland, 2000) and Natural (Krinov, 1947), which contain measurement of 'natural' surfaces, and a set of 1269 samples from the Munsell Book of Color (Parkkinen, 1989). The high degree of correlation seen in the SOCS data is again present, although each dataset has its own specific correlation profile.

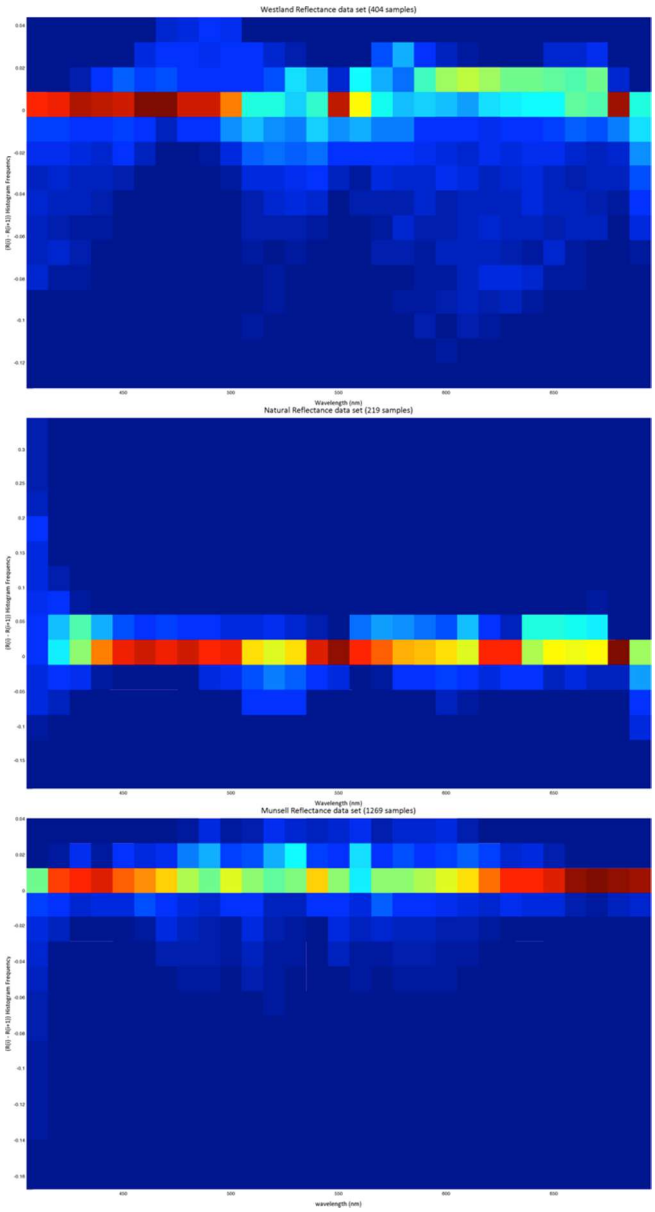


***Figure 6**. Top to bottom: Westland, Natural and Munsell datasets shown as per-wavelength histograms of the range of differences between $R(\lambda^i)$ and $R(\lambda^{i+1})$ without the top/bottom 5% of the range difference data in each set respectively.*

The following section shows how, given such characterization of a dataset, it is possible to re-create it synthetically from first-principles while maintaining its correlation profile. This allows for a computational design of datasets, following simple rules that can be established without the need for large numbers of manual measurements. For instance, given the set of spectral reflectances of individual Neugebauer Primaries (ink overprint combinations), it is possible to algorithmically generate a sampling of all possible reflectances that their combinations can give rise to.

## Spectral synthesis from correlation

The task of generating natural reflectances, i.e. reflectances that are like those found in nature, as characterized by a given set of features – either derived from measurements or defined *a priori*, can be approached from a variety of angles. Ultimately such synthetic generation of natural-like spectra has the aim of representatively sampling a small sub-space of the spectral domain, delimited at least by constraints on physical realisability (all reflectances falling within the [0 1] range), or further constraints dictated by properties of measured data. In the latter case the task is first to extract such fundamental measured data properties.

Multivariate analysis aims to find the principal axes of variation in a dataset, called principal components or characteristic vectors, which define a coordinate system that is de-correlated and is better suited to representing the data. Here "better suited" means representing data in a dimensionality-optimal way. However, the challenge is to know how representative measured datasets are. The aforementioned principal components are closely tied to the frequency of occurrence of data. A dataset containing 99 identical reflectances and 1 different one will have the first principal component match the 99 reflectances exactly as that is the principal direction present in the data. However such a dataset could also be treated as only 2 reflectances, in which case the first principal component would be very different. In measured datasets, that aim to be representative of some environment, this is a crucial question to address.

Another approach would be to consider a delimiting envelope of the dataset and sample the interior. This could be done for example by means of the convex hull in the reflectance domain (e.g. 16D for 400nm to 700nm at 20nm intervals, or 31D for the same range at 10nm intervals). Once a convex hull is obtained, the challenge is one of sampling it in a representative manner. Given the dimensionality of the convex hull, and it being a sub-polytope of the [0 1] hypercube, this is simple in principle but computationally expensive. A straightforward uniform sampling approach would result in the vast majority of samples being outside the spectral gamut. Likewise, a random generation of samples in the [0 1] hypercube range would also likely yield many out-of-spectral-gamut samples, rendering it similarly inefficient.

While the above approaches are certainly valid, the spectral correlation analysis shown in the previous section enables a new way to address this challenge. Here the core idea is that the spectral correlation in a dataset expresses the magnitude and direction of differences between consecutive wavelengths. Let these be denoted as a sequence of $\lambda^i_{min}$ and $\lambda^i_{max}$ for a given wavelength $\lambda^i$ defined as:

$$\lambda^i_{min} = \min_\lambda [\lambda^i - \lambda^{i+1}]$$

$$\lambda^i_{max} = \max_\lambda [\lambda^i - \lambda^{i+1}] \quad (1)$$

The set of $\lambda^i_{min}$ and $\lambda^i_{max}$ are per-wavelength ranges of differences between neighboring wavelengths taken over an entire dataset. These $N_{smp} - 1$ values, where $N_{smp}$ is the number of spectral intervals samples (e.g., 16, 31, …), determine the correlation profile of the dataset. Without loss of generality, let $[\lambda^i_{min}, \lambda^i_{max}]$ have been suitably filtered to discount outliers or measurement noise, as outlined in the previous section. The constraints for a synthesis from this correlation profile also have to satisfy physical realisability, hence any reflectance at $\lambda^i$ that differs from its previous wavelength by up to $[\lambda^i_{min}, \lambda^i_{max}]$ and lies within the range of [0 1] is considered a feasible sample.

The aim of synthesizing reflectances according to the spectral correlation profile is to define a generating set that is characteristic of an original correlation profile. The set should therefore describe the original assumptions of correlation and not give up any other properties it may have such as gamut or dimensionality. In both

cases a determining factor is spectral variation, hence it is not so much an objective to uniformly sample the correlation profile space, but rather sample it descriptively (i.e. maintaining the correlation profile and being representative of dimensionality and gamut).

Without loss of generality a 400nm to 700nm range at 20nm steps resulting in 16 spectral samples per reflectance is used here. The correlation profile is then described by a 15 x 2 matrix of $[\lambda^i_{min}, \lambda^i_{max}]$ values per wavelength as shown above in Eq. (1). For a simple case where both min and max are fixed and constant at 0.1 along the wavelength range Fig. 7 shows an example of reflectances that satisfy both the constraint of correlation and physical realisability.

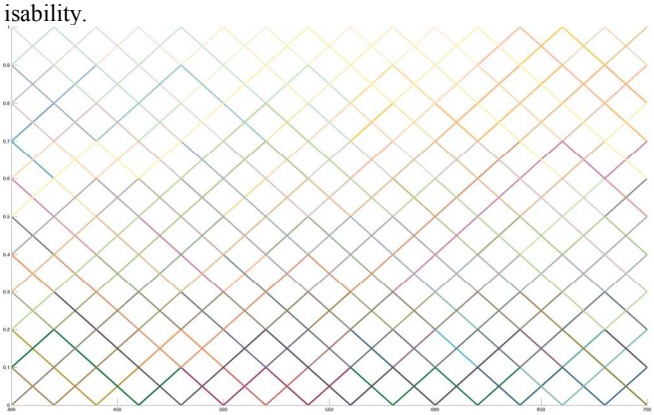

***Figure 7**. Synthetic reflectances with constant, wavelength independent correlation of 0.1.*

The per-wavelength correlation profile of the above data set is then shown in Fig. 8, and as expected shows a synthetic and regular distribution (compare against that of the SOCS data set in Fig. 2).

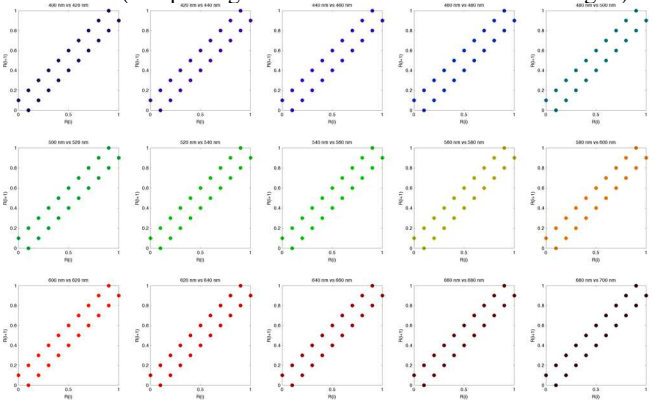

***Figure 8**. Per-wavelength correlation plot of synthetic reflectances with constant, wavelength independent correlation at 0.1.*

In Fig. 7 the initial seed for generating the reflectances were values of [0, 0.2, 0.4, 0.6, 0.8, 1] at 400nm and each subsequent wavelength was then generated as follows:

$$R(\lambda^{i+1}) = \begin{bmatrix} R(\lambda^i) & \left[R(\lambda^i) + \lambda^i_{max}\right] \\ R(\lambda^i) & \left[R(\lambda^i) - \lambda^i_{min}\right] \end{bmatrix} \quad (2)$$

where $R(\lambda^i)$ is the set of all partial reflectances up until $\lambda^i$ (i.e. $\lambda^i$ □400nm, R$(\lambda^i)$□ □̃ □̃ □̃ □̃ □̃ □̃ ı□̃. So, each set of values at a subsequent wavelength branches in two directions, one in the max-direction and one in the min-direction, much like a binary tree would. Starting with a single value, the tree would result in 216 leaves that each represent a different reflectance branch, so in the above example, having started from six uniformly distributed values in the [0, 1] interval the total number of branches is $6*2^{16}$ = 393,216. However some of these are not valid reflectances and exceed the [0 1] interval (e.g. starting at 1 the only possible branch is the min-branch, etc.). Such branches are pruned at each wavelength and reduce the complexity of the computation both in speed and in memory requirement. Once the last wavelength is computed, the same process is done in reverse order, starting from the initial seed values at 700nm and computing all branches down to 400nm with the ranges inverted, as follows:

$$R(\lambda^{i-1}) = \begin{bmatrix} \left[R(\lambda^i) - \lambda^i_{max}\right] & R(\lambda^i) \\ \left[R(\lambda^i) + \lambda^i_{min}\right] & R(\lambda^i) \end{bmatrix} \quad (3)$$

In this synthetic example with a constant, wavelength independent correlation difference where for all $i$ [$\lambda^i_{min}$ = -0.1, $\lambda^i_{max}$ = 0.1] the total number of reflectances after pruning is 187,440 which is just under half of all generated samples and the time to generate this entire set is ~140 ms on a 2.66 GHz Intel Core i7 with 8GB RAM.

For a real-world example instead, the correlation profile of the SOCS data set is used below to generate reflectances as outlined above. The filtered correlation profile here is that shown in Fig. 3 above and Fig. 9 shows the 'forward' direction (Formula (2)) and 'reverse' direction (Formula (3)) of the synthesized reflectances.

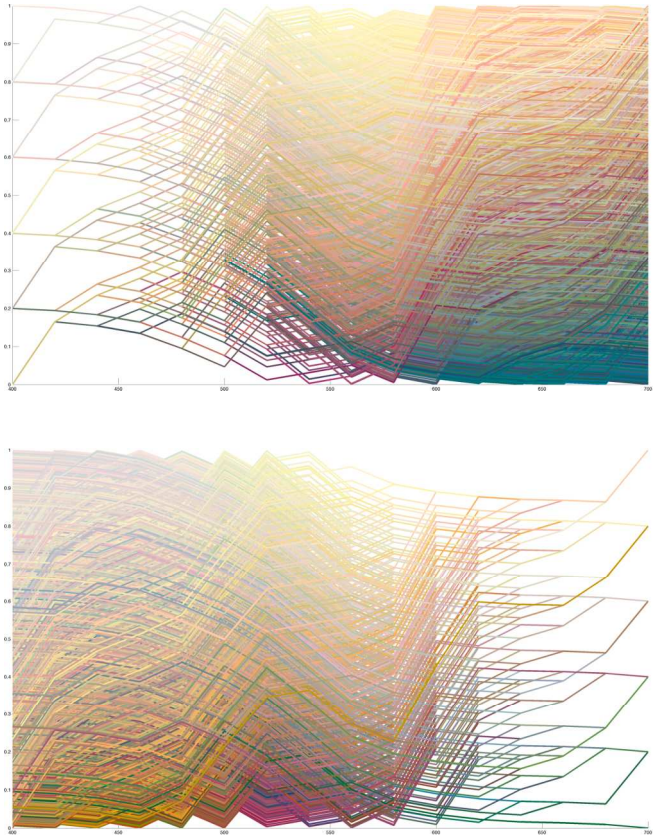

***Figure 9**. Forward (top) and reverse (bottom) direction of synthesized reflectances based on the SOCS correlation profile.*

Unlike the choice of initial seed values at wavelengths $\lambda^1$ and $\lambda^N$, only representing the extremes of the correlation ranges is not arbi-

trary. Given a set of reflectances and all combinations of per-wavelength extreme values, these reflectances are sufficient to describe the set fully by virtue of the preservation of convexity between the reflectance domain and colorimetry. Since colorimetry is a linearly weighted sum over all wavelength samples, any sample that can be expressed as a weighted (convex) linear combination of any number of base reflectances is contained in terms of the spectral and color gamuts of that set. Hence in this way a linear model basis, not to be mistaken for a PCA based linear model basis, can be generated that inherently contains the per-wavelength correlation properties and completely describes the color and spectral gamuts. A PCA based linear model basis can be thought of as the opposite of this correlation approach. The correlation method delimits the spectral and color gamuts, while PCA maximizes decorrelation without heed for gamut.

This min/max representation also deliberately ignores the intra-wavelength distribution of the range since that is related to the actual samples taken in a dataset (see the earlier example of 99 equal reflectances and one different one) rather than intrinsic correlation properties.

Thanks to such per-wavelength convexity, combinations of per-wavelength extremes both in relative (with respect to previous and subsequent wavelengths) and absolute terms (the absolute reflectance factors possible) can be generated in the following constructive approach to building a basis:

1. For each $\lambda^j$ in the range of $[\lambda^1 = 400, \lambda^N = 700]$nm:
2. Start at wavelength $\lambda^j$ with an initial seed of [0 1], the two extremes of physical realisability.
3. Build a left-to-right binary tree based on $[\lambda^i_{min}, \lambda^i_{max}]$ for $i > j$ based on Formula (2) and a right-to-left binary tree based on $[\lambda^i_{min}, \lambda^i_{max}]$ for $i < j$ based on Formula (3).
4. Prune both left-to-right and right-to-left branches to satisfy the physical realisability constraint.
5. For each partial reflectance from the right-to-left branch combine with all reflectances with the left-to-right branch to create a full set of reflectances for $\lambda^j$.

The above procedure results in an exhaustive, fully descriptive set of reflectances that envelopes the original data set defined by the $[\lambda^i_{min}, \lambda^i_{max}]$ ranges. Fig. 10 shows the first two such data sets starting at 400nm and 700nm using the SOCS correlation profile.

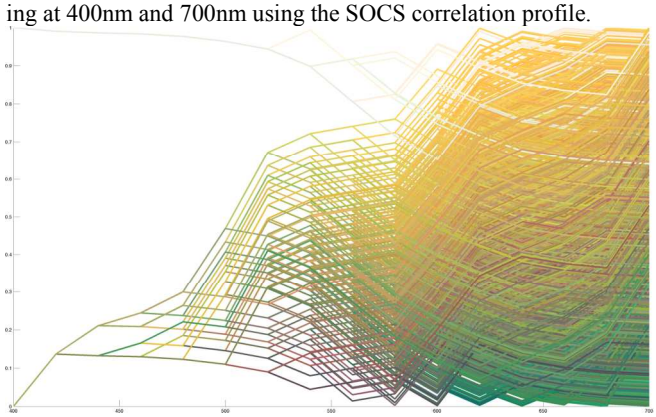

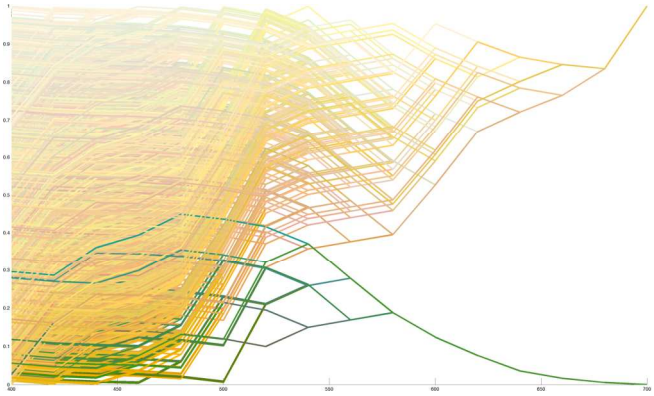

***Figure 10**. Synthesized reflectances based on the SOCS correlation profile for initial seed values of [0 1] at 400nm (top) and 700nm (bottom).*

The above approach enables the sampling of spectral data based on *a priori* information in the form of spectral correlation and does so without the sampling bias likely present in measured data sets. The approach is systematic and efficient compared to other methods that either sample large domains of spectral space that are invalid (out of spectral gamut), do so non-uniformly, or take into account the frequency of measured data that need not be meaningful.

## Comparison of measured and synthetized spectra

The first type of comparison that can be made between synthesized and measured reflectances is directly in terms of their correlation profiles. Taking the reflectances generated to match the SOCS dataset's profile (Fig. 9) and performing the same correlation analysis as shown in the previous section, the profile (Fig. 11 bottom) matches exactly that of the SOCS data. This comes as no surprise since it is the correlation profile that is the principle of synthesis here.

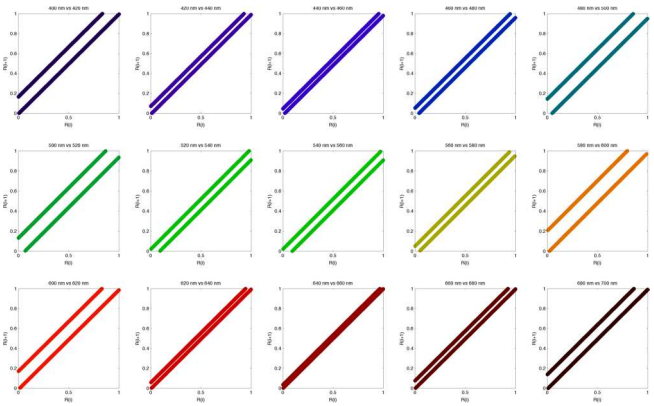

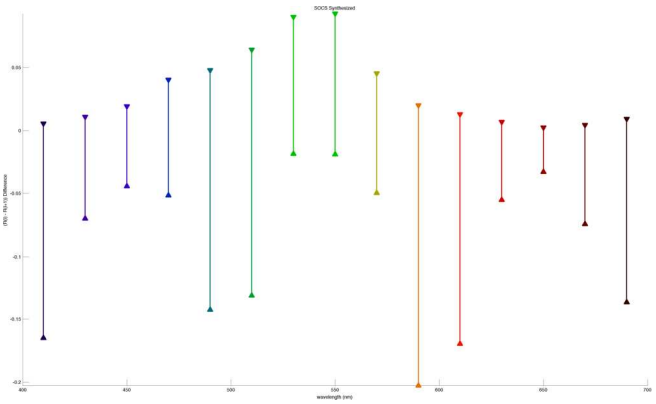

***Figure 11**. Per wavelength reflectance differences (top) and per wavelength range of differences (bottom) of the synthetically generated reflectances, based on the SOCS correlation profile.*

Fig. 10 also shows that an even closer match to the original data set can be had if the per-wavelength absolute reflectance values are also considered. To do so both $[\lambda^i_{min}, \lambda^i_{max}]$ of neighboring wavelength correlation as well as $[\lambda^i_{min}, \lambda^i_{max}]$ of absolute reflectance values that serve as per wavelength seeds are needed. Results using this approach will be shown in the final paper.

Second, it is also possible to consider the measured and synthetic spectra from the perspective of multivariate analysis and to compute their principal component bases. Fig. 12 therefore shows the first five SOCS bases both for the measured (accounting for 99.7% variance) and the synthetic data (accounting for 99.8% variance).

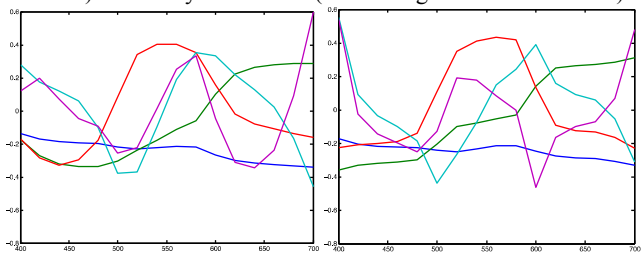

***Figure 12**. PCA bases of measured (left) and synthetic (right) SOCS spectra.*

For comparison, Fig. 13 shows the same analysis for the 1269 Munsell spectra, where the first five bases account for 99.9% of the measured and 99.6% of the synthetic dataset's variance.

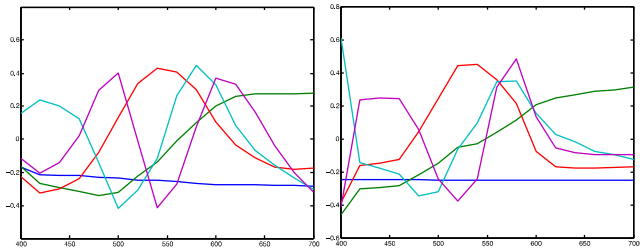

***Figure 13**. PCA bases of measured (left) and synthetic (right) Munsell spectra.*

While the bases aren't identical for either dataset, they show a great deal of similarity with the measured-synthetic relationship being clearly closer than that of the two measured datasets. The source of their differences also follows from how the synthetic data is generated, where it is not its intent to match the measured data but effectively to sample the full gamut of all spectra that have the measured dataset's correlation profile. That the gap is greater for the Munsell than the SOCS data is also consistent with the former dataset both being smaller and having a smaller gamut.

Finally, it is also worth computing the PCA bases of the spectra synthetized for a 'flat' correlation profile, like the one shown in Figs. 7 and 8 where the correlation bounds are a constant ±0.1. Fig. 14 therefore shows the first five bases of that set of correlation-synthetizes spectra, which account for 99.1% of their variance.

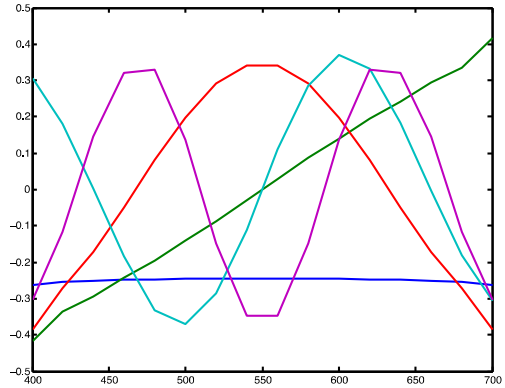

***Figure 14**. PCA bases of spectra synthesizes using a constant ±0.1 correlation profile.*

The bases in Fig. 14 resemble those of a sine basis, as also used in the Fourier series. This can be read as it being the specific correlation profiles of natural spectra that account for their shapes being other than those of simple sine/cosine functions. How the correlation profile relates to the derived PCA basis in general is another area of future investigation.

## Conclusions

The correlation method of spectral reflectance synthesis presented here is a fundamental alternative to methods using the bases derived from multivariate analysis. Instead of de-correlating spectra, it starts from a characterization of a spectral dataset's correlation profile and then applies it as parameters for direct wavelength to consecutive wavelength synthesis. The end result is a set of spectra that directly and fully sample spectral and colorimetric gamut of a spectral dataset in an efficient way.

In terms of next steps, spectral synthesis from correlation can be applied to Bayesian models like those presented by Brainard *et al.* (2006), with the correlation profile acting as a prior, which – unlike a convex hull spectral gamut – is applicable at a pixel level, and with the model's output being spectral reflectance in its full dimensionality. As far as the method itself is concerned, it would also be possible to extend it by adding a specific sampling of the base reflectances whose generation was described here, e.g., following a Gaussian distribution between min-max extremes considered here. The synthesized reflectances generated in this way could also be further constrained by the *naturalness constraint* (a convex combination of measured natural reflectances is also a natural reflectance) as presented by Morovič (2002) which would bound the synthesized reflectances to the convex hull of the originating data sets, if that is desired, while still maintaining the spectral correlation profile.

## Acknowledgements

The authors would like to thank the following colleagues for their support: David Gaston, Carlos Amselem and Rafael Giménez.

## References

Brainard DH, Longère P, Delahunt PB, Freeman WT, Kraft JM, Xiao B (2006) Bayesian model of human color constancy, J Vis, November 6, 2006 6(11): 10; doi:10.1167/6.11.10

Chau WWK, Cowan WB (1996) Gamut Mapping Based on the Fundamental Components of Reflective Image Specifications, Proceedings of 4th IS&T/SID Color Imaging Conference, pp. 67–70.

Cohen J (1964) Dependency of the spectral reflectance curves of the Munsell color chips, Psychonomic Science, Vol 1(12), 1964, 369-370.

Kohonen O, Parkkinen J, Jääskeläinen T (2006) Databases of Spectral Color Science, Color Research and Application, 31(5):381-389.

Krinov EL (1947) Spectral Reflectance Properties of Natural Formations, Proceedings of the Academy of Sciences of the USSR.

Morovič J, Cheung V, Morovič P (2012) Why We Don't Know How Many Colors There Are, CGIV, May 6–9, Amsterdam, The Netherlands, pp. 49-53.

Morovič P, Finlayson GD (2006) Metamer-set-based approach to estimating surface reflectance from camera RGB, JOSA A 23 (8), 1814-1822.

Morovič P (2002). Metamer Sets, PhD Thesis at University of East Anglia.

Parkkinen JPS, Hallikanen J, Jaaskelainen T (1989). Characteristic spectra of munsell colors. JOSA A, 6:318–322.

Schrödinger E. (1920) Theorie der Pigmente von größter Leuchtkraft, Annalen der Physik (Paris), vol. 62, pp. 603-622.

Singh B, Freeman W, Brainard D (2003) Exploiting Spatial and Spectral Image Regularities for Color Constancy, *Proc. Workshop Statistical and Computational Theories of Vision,* 2003.

Smith MO, Johnson PE, Adams JB (1985) Quantitative determination of mineral types and abundances from reflectance spectra using principal components analysis, Proc. 15th Lunar and Planetary Sei. Conf., Part 2, Geophys. Res., vol. 90, suppl., pp. C797-C804, Feb. 15, 1985.

Tkačik G, Garrigan P, Ratliff C, Milčinski G, Klein JM, Seyfarth LH, Sterling P, Brainard DH, Balasubramanian V (2011) Natural Images from the Birthplace of the Human Eye. PLoS ONE 6(6): e20409. doi:10.1371/journal.pone.0020409

Westland S, Shaw J, Owens H (2000). Colour statistics of natural and man-made surfaces. Sensor Review, 20(1):50– 55.

## Author Biography

*Peter Morovic received his Ph.D. from the University of East Anglia, UK in 2002 and holds a B.Sc. in theoretical computer science from Comenius University, Slovakia. He has been a Color and Imaging Scientist at Hewlett–Packard, Spain since 2007. His research interests include color reproduction, image processing and computational geometry; he received the IS&T's Raymond Davis Scholarship (2001) and the JSPS Post–doctoral Fellowship (2005).*

*Ján Morovic received his Ph.D. in color science from the Colour & Imaging Institute of the University of Derby (UK) in 1998. After working there as a lecturer in digital color reproduction, he became senior color scientist and later master technologist at Hewlett-Packard in Barcelona, where he has been since 2003. He is also the director of the CIE's Division 8 on Image Technology and Wiley and Sons have published his 'Color Gamut Mapping' book.*

*Juan M. García-Reyero received his Ph.D. from the Politechnical University of Catalonia (UPC, Spain) in 2000, and holds an MD in Mechanical Engineering from UPC. He has worked as an engineer specializing in inkjet writing systems at Hewlett-Packard in Barcelona since 1996. In 2008 he became an HP Master Technologist.*